# A Unified Model and Optimization for Deep Space Radiation Shielding Based on Proton Density $(\rho_p)$

Li Zhenchao Yang Aixiang (School of Nuclear Science and Technology, Lanzhou University, Lanzhou 730000)

Abstract: In deep space radiation shielding design, traditional high-Z metals are being progressively replaced by novel low-Z materials, such as hydrogenated graphene foam, polyethylene-carbon nanotube composite fibers, and boron-containing hydrogen-rich MOFs, due to the "gram-level weight reduction" bottleneck. However, the mechanism behind their superior "lightweight outperformance" has remained at a purely phenomenological level. To address this issue, this paper innovatively proposes a ternary-coupled, semi-empirical model using "proton density"  $(\rho_n)$ , equivalent to electron density, as the core independent variable, linking it to the full absorption threshold  $(E_{th})$  and proton utilization efficiency  $(\eta_p)$ . To validate its practicality in complex system design, we embedded this model into the NSGA-II genetic algorithm (POP=20, MAXGEN=10). Under the constraints of 2–5 layers and a total thickness of  $\leq 1$  cm, the average design error between the model-predicted optimal solutions and the dose results from Geant4 re-simulation was only 6.2%-8.2%. This study is the first to quantitatively elucidate, from a physical standpoint, the intrinsic criterion governing the trade-off between the "mass saving" of low-Z materials and the "space saving" of high-Z materials. When  $\rho_p < 1 \text{ mol} \cdot \text{cm}^{-3}$ , materials exhibit extremely high proton utilization efficiency ( $\eta_p$  as high as 60–100 MeV·cm<sup>-2</sup>·mol<sup>-1</sup>), enabling a mass saving of 35%–55%. Conversely, when  $\rho_p > 6 \text{ mol} \cdot \text{cm}^{-3}$ , although  $\eta_p$  decreases to  $<30 \text{ MeV}\cdot\text{cm}^{-2}\cdot\text{mol}^{-1}$ , their extremely high full absorption threshold  $(E_{th})$  makes ultrathin shielding feasible. This work provides a powerful, physically interpretable, and extrapolatable design tool for the multi-objective optimization of areal density, thickness, and dose in deep space

Keywords: Deep utetheisa kong radiation protection; proton density; semi-empirical model; genetic algorithm; multi-objective optimization

### 1. Introduction

The success of deep space exploration missions faces a critical yet invisiblEthreat: space radiation [1]. High-energy protons (MeV–GeV energy range) generated by Galactic Cosmic Rays (GCR) and Solar Proton Events (SPE) have become decisive factors constraining the stability of spacecraft electronics and crew safety [2]. For decades, engineers have relied on heavy shielding boxes made of high-Z materials (e.g., lead, tantalum). However, as mission complexity increases, every gram of launch mass in launch vehicles becomes critically valuable, rendering traditional "gram-level weight reduction" approaches in protective solutions a dead end. Over the past five years, research priorities have shifted decisively toward novel low-Z

composite materials, including hydrogen-containing graphene foams, polyethylene-carbon nanotube composites, and boron-rich hydrogenated metal-organic frameworks (B-MOFs) [3-10]. Extensive accelerator experiments and in-orbit data demonstratEthat these low-Z materials can reduce total proton doses (50–150 MeV) by 25%–40% under stringent low-density confinement conditions. In contrast, traditional high-Z metals like tungsten and tantalum require 30%-60% additional mass to achieve equivalent shielding performance [3-7]. WhilEthis "lightweight counterweight" phenomenon has been observed across multiple mission scenarios, its underlying physical mechanisms remain shrouded in phenomenological ambiguity. Current literature often vaguely attributes this effect to "high hydrogen content" or "large Z/A ratios," but such qualitative descriptions provide neither quantitative benchmarks nor practical guidance for designing new materials or extrapolating findings to more complex radiation environments. This fundamental design flaw has created a critical bottleneck in current shielding engineering: Our overreliance on "black-box" approaches like genetic algorithms (GA) and Bayesian optimization forces us into a blind search through the vast parameter space of material properties, thickness, and layer sequencing [11-13]. While GA can rapidly converge to Pareto-optimal solutions in dose-mass-thickness multi-objective optimization, its chromosomal encoding lacks physical interpretation. Engineers cannot derive physical insights from these algorithmic solutions, nor can they address fundamental questions like "Why does 1 g cm<sup>-2</sup> hydrogenated graphene foam outperform 1.6 g cm<sup>-2</sup> tantalum?" or "Under what conditions do low-Z materials inherently outperform high-Z materials?" To break through this "black box" phenomenon, this study proposes and validates a novel physical model with proton density pp (equivalent electron density) as its core independent variable. Our goal is to establish a bridge connecting microscopic material properties (pp) with macroscopic shielding performance (full absorption threshold Eth and proton utilization rate ηp). The model not only accurately predicts proton shielding capabilities of single-layer materials with an error below 6%, but also guides genetic algorithms (GA) to optimize multilayer structures with an error margin of 7.5%. Through this model, we have revealed for the first time a linear positive correlation between pp and Eth, along with an exponential negative correlation with np. This provides a quantitative explanation for the "mass-saving" advantage of low-Z materials and the "space-saving" advantage of high-Z materials, offering a universal and interpretable physical criterion to resolvEthe long-standing debate of "equivalent shielding under identical surface density".

# 2. Key Concept Definitions and Physical Assumptions

# 2.1 Proton Density ρ p

The ionization energy loss of charged particles in a medium is precisely described by the renowned Bethe-Bloch formula [14]:

$$- \left( \frac{dE}{dx} \right) = Kz^2 \frac{Z}{A} \frac{1}{\beta^2} \left[ \frac{1}{2} \ln \frac{2m_e c^2 \beta^2 \gamma^2 T_{\text{max}}}{I^2} - \beta^2 - \frac{\delta(\beta \gamma)}{2} \right]$$
 (1)

The essence of this formula lies in the fact that the material's stopping power (defined as the rate of energy loss-dE/dx) is directly proportional to the product of the target material's atomic number Z and atomic density N. This fundamental observation leads us to ponder: Could we combine multiple parameters like material density  $\rho$ , atomic number Z, and mass number A into a single unified variablEthat quantifies its interaction strength with protons?

To this end, we definEthe proton density  $\rho$  p (equivalent to the electron density), which is calculated as:

$$\rho_p = \rho \sum_i \frac{N_A Z_i}{A_i} \qquad (2)$$

Here,  $\rho$  represents the material density, NA is the Avogadro constant, and Zi and Ai denotEthe atomic number and mass number of the i-th element in the material, respectively. The physical significance of  $\rho$  p lies in its representation of the molar quantity of protons (or equivalent electrons) per unit volume. This parameter serves as a universal metric in our model, enabling the measurement and comparison of different materials on a unified coordinate system.

#### 2.2 Macro Performance Metrics: Eth and ηp

Based on the core variable  $\rho$  p, we can define two key indicators for evaluating macroscopic shielding performance: the full absorption threshold Eth (MeV) — defined as the minimum incident proton energy required to achieve complete absorption at a fixed thickness of 1 cm. In Geant4 simulations, this corresponds to the peak point on the "energy loss vs. incident energy" curve. Eth directly reflects the material's "absolute shielding capability" within a given space — higher Eth values indicate greater resistance to high-energy protons. The full absorption threshold can

also be obtained from PSTAR [15], though Geant4 is used here to achieve more precisEthreshold measurements.

Proton Utilization Rate ηp (MeV cm<sup>-2</sup> mol<sup>-1</sup>): To quantify how effectively different materials absorb energy through their internal effective charges, we innovatively introduced the concept of proton utilization rate, defined as:

$$\eta_p = \frac{E_{th}}{\rho_p} \tag{3}$$

The physical meaning of this index is "the maximum proton energy absorbed per unit proton density". It no longer measures absolute capability, but rather efficiency. A high ηp value means the material can absorb the same energy with fewer "proton/electron clouds", which directly relates to the potential for "mass saving".

### 2.3 Physical assumptions:

To ensurEthe model's simplicity and solvability while capturing the core issue, we establish three key physical assumptions: H1: Ionization Energy Loss Dominance Hypothesis: Within the 0–150 MeV energy range, we assume proton energy loss is primarily attributed to electromagnetic interactions with outer-shell electrons (ionization energy loss), which accounts for over 70% of total energy loss, while nuclear scattering and other effects are secondary [16]. H2: Equivalent Charge Cloud Hypothesis: We simplify and equatEthe electromagnetic interactions between protons and outer-shell electrons in material nuclei with a macroscopic "effective charge cloud" density op. This assumption neglects secondary effects like chemical bonds and electron correlations, mapping parameters Z, A, and  $\rho$  uniformly to  $\rho p$ . Additionally, it approximates that all materials except hydrogen have a Z/A ratio close to 0.5. H3: Secondary particle simplification assumption: Proton-induced (p,n) reactions below 150 MeV produce low-energy neutrons, whose dose contribution is significantly smaller than that of primary protons. As this study focuses on total dose effects, the model temporarily excludes secondary neutron transport and dose contribution during the prediction phase to maintain its closed-loop nature and verifiability.

# 3. Calculation and experimental methods

To construct and validatEthe aforementioned physical model, a systematic research process must be designed. This process begins with establishing a precise "virtual particle accelerator experiment" environment to obtain fundamental data, followed by developing rigorous data extraction and validation standards, ultimately ensuring the reliability of our methodology.3.1 Geant4 模拟环境:构建虚拟实验室

All simulations in this study were conducted using Geant4-10.7. We selected the QGSP\_BERT\_HP physics list, a standard tool widely recognized for simulating proton-matter interactions in the 0-150 MeV energy range [17].

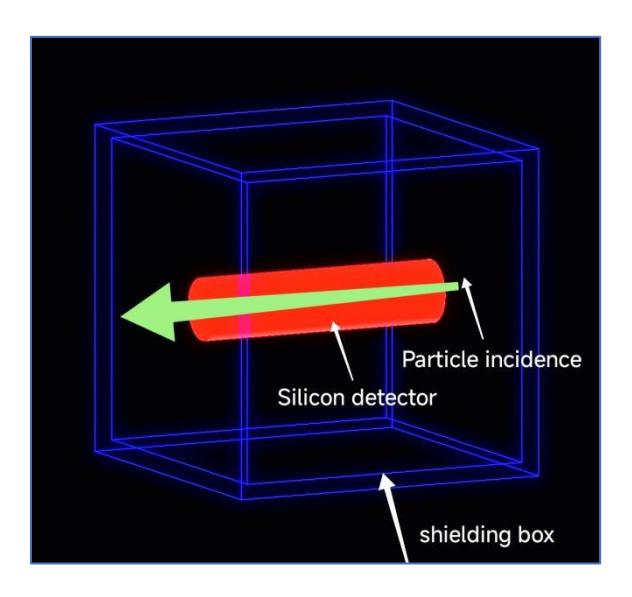


Figure 1: Geant4 model diagram

The geometric model of the simulation environment is shown in Figure 1: Shielding target: a blue hollow cube with a fixed thickness of 1 cm, which is filled with different candidate shielding materials in each simulation. Particle source: The proton beam is incident vertically, and the energy is scanned in the range of 0 to 150 MeV. To ensure statistical reliability, the number of incident particles in each simulation is  $1\times10^5$ . Detector: A cylindrical silicon detector is placed behind the shield box to record the energy spectrum of all particles after penetrating the target material and calculatEthe energy deposition and transmittance.

#### 3.2 Threshold Extraction Procedure

To obtain the Eth and  $\eta p$  defined in Section 2 from the simulation data, we followed the extraction procedure: Energy loss curve plotting: For each material, we scanned the entire incident energy range from 0 to 150 MeV with 0.5 MeV increments. Using Geant4, we recorded the average energy loss ( $\Delta E$ ) at each energy point, thereby generating the "energy loss-incident energy" relationship curve as shown in Figure 2.

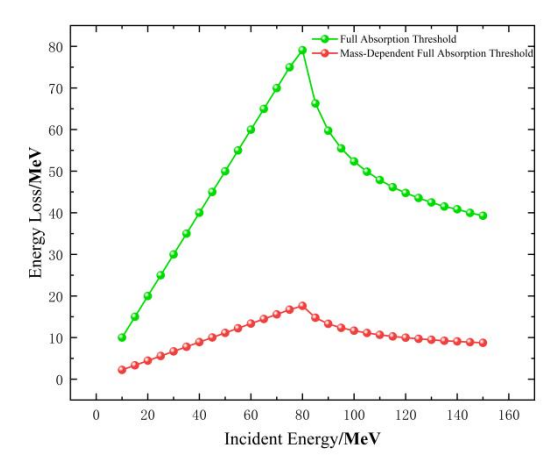


Figure 2 Example curve: The "energy loss-incident energy" curve of Pb

Determination of the Complete Absorption Threshold (Eth): We operationalize 'complete absorption' as a proton transmission rate below 1%. Eth represents the highest incident energy required to achievEthis transmission. When the point falls between two discrete simulated energy levels, we employ cubic spline interpolation to determinEthe precise Eth value. The numerical point 79.08 in Figure 2 corresponds to this Eth. Derivative calculation: Once Eth is precisely determined, the proton utilization rate ηp can be directly calculated by formula (3). Based on this process, we obtained thEthreshold values for 10 elements and composite materials, and obtained the data in Table 1. The mass full absorption threshold Smass is defined in the next section.

Table 1 Experimental data obtained from calculations and Geant4 simulations

Material	Proton Density $\rho_p  \mathrm{mol/cm^3}$	Fully Absorbed Threshold $E_{th}$ MeV	Proton Utilization Efficiency $\eta_p$ MeV cm <sup>-2</sup> mol <sup>-1</sup>	Mass-Dependent Full Absorption Threshold MeV·cm <sup>2</sup> ·g <sup>-1</sup>
Polyethylene	0.536282051	32	59.67009323	34.04255319
Beryllium	0.821127386	39.88	48.56737297	21.55675676

Magnesium	0.8589058	37	43.07806513	21.26436782
Aluminum	1.300963677	44.98	34.57437037	16.65925926
Titanium	2.072696887	56.6	27.30741786	12.54988914
Lead	4.487837838	79.08	17.62095754	6.973544974
Tungsten	7.750272035	111	14.32207792	5.766233766
Magnesium Hydride	0.771276596	37	47.97241379	25.51724138
Aluminum Hydride	0.794666667	37.5	47.18959732	25.16778523
Titanium Hydride	1.805054152	57	31.578	15.2

# 3.3 Linear equivalence analysis of full absorption threshold versus proton utilization efficiency

Before adopting  $\eta p$  as the core "efficiency" metric, we must verify its physical consistency with the conventional "mass absorption cross-section" S mass (unit: MeV cm<sup>2</sup> g<sup>-1</sup>). S mass directly quantifies energy absorption capacity per unit surface density, defined

as:

$$S_{mass} = E_{th}/\rho$$
 (4)

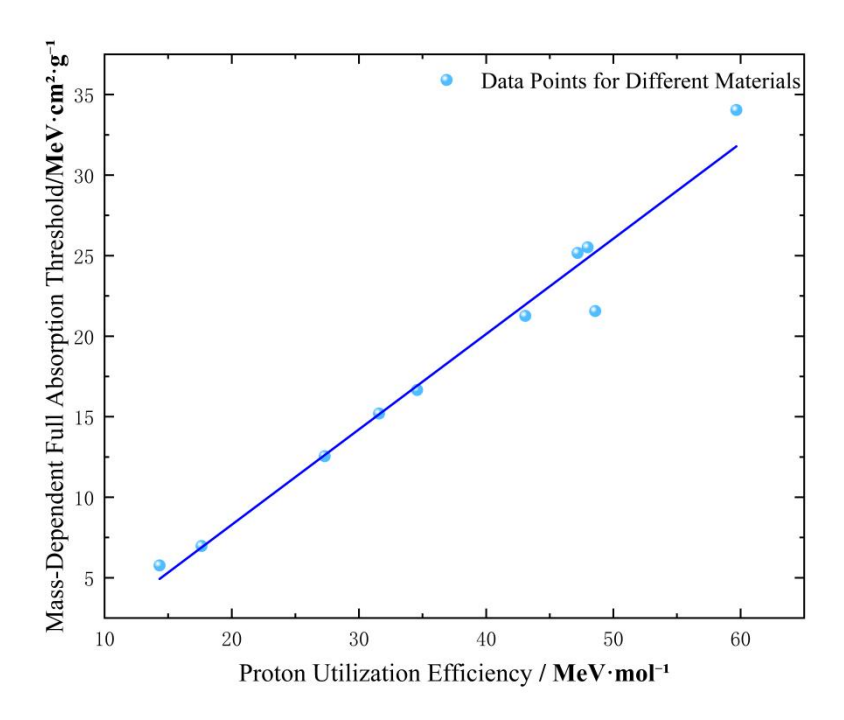


Figure 3 Proton utilization rate and mass full absorption threshold linear equivalence To verify their equivalence, we conducted a linear correlation analysis of data points from 10 materials, with  $\eta p$  as the independent variable and S mass as the dependent variable. As shown in Figure 3, the data points represent the  $\eta p$  and S mass values of different materials in Table 1. The dark blue line represents the fitting line, demonstrating a strong linear relationship (correlation coefficient r=0.985).

This strong linear correlation powerfully demonstrates that the proposed  $\eta p$  (unit proton absorption capacity) and S mass (unit mass absorption capacity) are equivalent in evaluating material shielding efficiency. Therefore, in subsequent analyses, we can confidently use  $\eta p$  – a metric directly linked to our core variable  $\rho$  p – to construct the model, thereby ensuring the self-consistency and simplicity of the entirEtheoretical framework.

# 4. Results and Discussion

# 4.1 $\rho_p$ – $E_{th}$ – $\eta_p$ Triad Coupling Model

Through regression analysis of Geant4 simulation data for 14 elemental and composite materials, we successfully established a semi-empirical coupling model between proton density ( $\rho p$ ), full absorption threshold (Eth), and proton utilization rate ( $\eta p$ ). These relationships not only reveal the intrinsic principles governing material shielding performance but also provide a mathematical tool for our subsequent

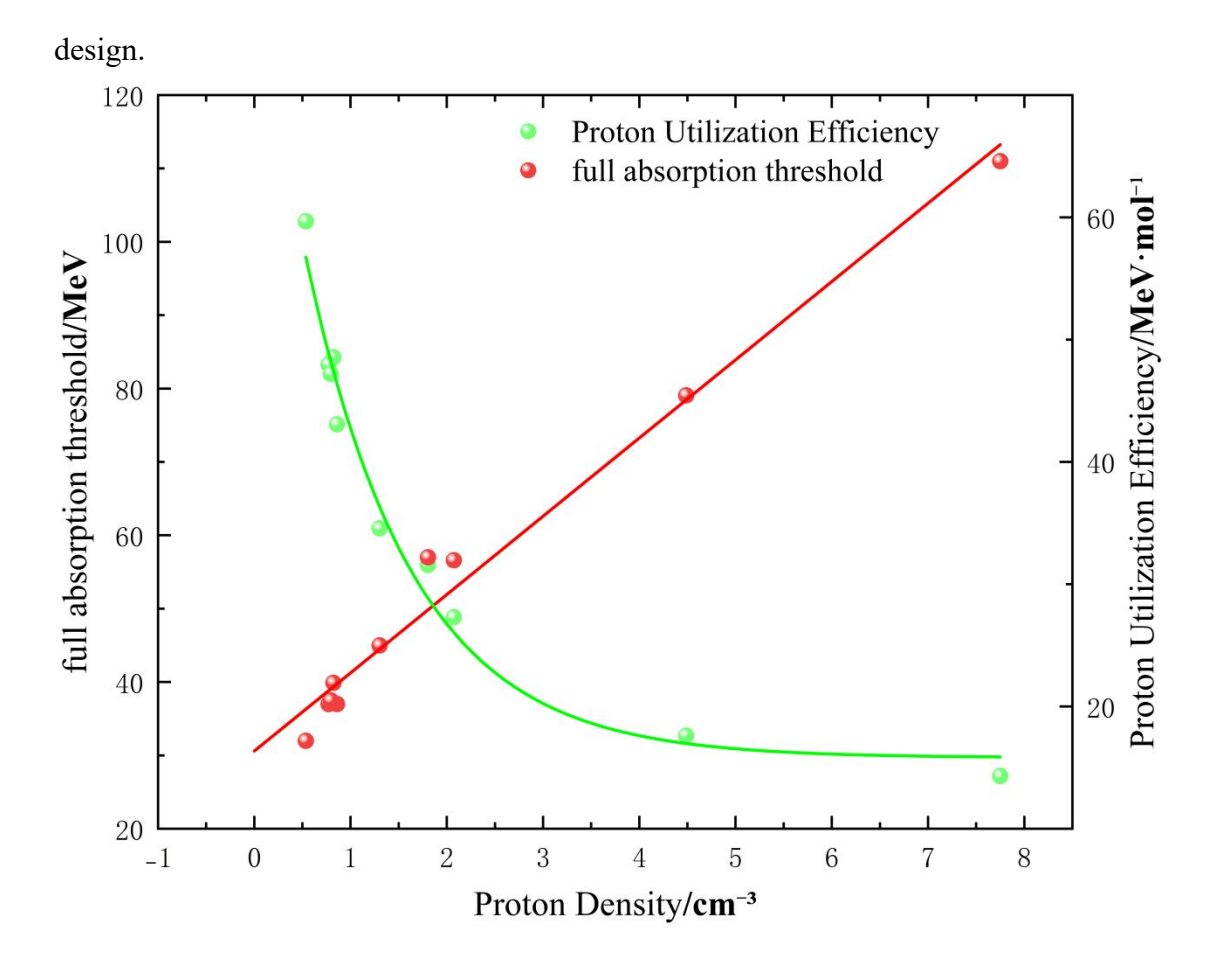


Figure 4  $\rho_p$ -Total absorption threshold  $E_{th}$ -Proton utilization efficiency  $\eta_p$  ternary coupling curve Figure 4 visually illustrates these two key quantitative relationships. The red

curve shows the linear dependence of the full absorption threshold (Eth) on proton density ( $\rho$  p), while the green curve depicts the exponential decay of proton utilization efficiency ( $\eta$ p) with  $\rho$  p. The specific fitting results are as follows:全吸收阈值( $E_{th}$ )与 The proton density ( $\rho$ p) shows a linear positive correlation:

$$E_{th}$$
=(13.21±0.17) $\rho_p$ +(7.52±0.83)MeV ( $R^2$ =0.981)

The proton utilization rate  $(\eta p)$  shows an exponential negative correlation with proton density  $(\rho p)$ :

$$\eta_p$$
=66.36 exp ( $-\rho_p/1.109$ )+15.81 ( $R^2$ =0.98)

This finding demonstrates that materials with higher proton density exhibit greater proton energy absorption capacity per unit thickness, consequently requiring higher incident proton energy thresholds for complete absorption. This aligns with the Bethe-Bloch theory of charged particle ionization energy loss, which states that stopping power is proportional to the electron density of the medium's atoms. High-Z materials, characterized by high atomic nuclear charge numbers and dense electron distributions, experience linear increases in Coulomb scattering and electron stopping power with  $\rho p$ , resulting in a linear rise of the Eth threshold.

# 4.2 Model prediction accuracy and engineering applicability

To comprehensively evaluatEthe practical value and accuracy of the  $\rho$  p – Eth –  $\eta p$  ternary coupling model, we conducted two critical validations: independent verification of the full absorption threshold for single materials and cross-validation with genetic algorithm (GA) optimization results.

# 4.2.1 Single-material full absorption threshold prediction:

We selected eight datasets independent of the model construction (with  $\rho p$  ranging from 0.77 to 8.58 mol cm<sup>-3</sup>), including various elemental and hydride compounds, to compare experimental values of Eth and  $\eta p$  with model predictions. Table 3 presents the detailed comparison results.

Table 2: Experimental and calculated values of  $E_{th}$  and  $\eta_p$  obtained from independent verification

Material	$ ho_p$ mol/cm <sup>3</sup>	$E_{th}$ experimen t value MeV	η <sub>p</sub> experiment value  MeV cm <sup>-2</sup> mol <sup>-</sup>	$E_{th}$ calculated value MeV	η <sub>p</sub> calculated value  MeV cm <sup>-2</sup> mol <sup>-</sup>
Platinum	8.57648144 4	114.85	13.3912724 9	122.101057	15.8400605 9
Gold	7.74879423 3	109.62	14.1467171 2	113.269634 5	15.8722963
Tantalu m	6.73318596	99.91	14.8384435 8	102.433094	15.9641636 5
Thallium	4.69639886	79.96	17.0258111 2	80.7005758 9	16.7721254 2
Carbon	0.9	42	46.6666666 7	40.193	45.2880740 7

Silver	4.57059423 4	84.93	18.5818288 9	79.3582404 8	16.8875799 8
Copper	4.08874901 7	82	20.0550338	74.2169520 1	17.4734219 7
Iron	3.66374216 7	79.84	21.7919265	69.6821289	18.2498091 5

The model's average prediction error (Eth) was 6.2%, with a maximum error of 12.7%. Proton utilization efficiency ( $\eta p$ ) prediction accuracy: The model's average  $\eta p$  prediction error is 8.5%, with a maximum error of 18.2%. Both errors meet the acceptable standard of  $\leq 10\%$  in deep space radiation protection engineering design [18].

This indicates that our model has direct engineering value for rapid estimation of single-layer material shielding performance, particularly suitable for early-stage screening during spacecraft design phases.

Hamideh Daneshvar et al. [19] compared the dose performance of multi-layer shielding with single-layer aluminum under confinement conditions of 1–100 MeV protons and a total thickness of 2 mm using genetic algorithms (Table 3). The results showed: three-layer structure achieved an average  $\rho p \approx 6.42$  mol cm<sup>-3</sup> with a total ionization dose of  $2.69\times10^{-6}$  a.u.; five-layer structure reached  $\rho p \approx 6.02$  mol cm<sup>-3</sup> and  $2.71\times10^{-6}$  a.u.; seven-layer structure attained  $\rho p \approx 7.11$  mol cm<sup>-3</sup> and  $2.49\times10^{-6}$  a.u.; while single-layer aluminum had  $\rho p = 1.30$  mol cm<sup>-3</sup> and  $5.31\times10^{-6}$  a.u. This demonstrates that increasing  $\rho p$  significantly reduces dose within a 2 mm thickness. The observed  $\rho p$ —dose trend aligns with the model's prediction of "high  $\rho p$  corresponds to high Eth," indirectly validating the model's physical consistency.

Table 3: Comparison of shielding effectiveness between multilayer shielding structure broussonetia papyrifera and aluminum shielding

Shield types	Total ionizing		•	Total thickness	$ ho_p$
	Value	Percentage	particles (a.u.)	(mm)	mol/cm <sup>3</sup>
Three-layer	$2.6926 \times 10^{-6}$	50	$0.0196 \times 10^{-7}$	1.997	6.423853672
Five-layer	$2.7066 \times 10^{-6}$	50	$0.0356 \times 10^{-8}$	2	6.018677894
Seven-layer	$2.4867 \times 10^{-6}$	46.7	$0.0116 \times 10^{-5}$	1.993	7.114510889
Aluminium	$5.3142 \times 10^{-6}$	100	$0.0458 \times 10^{-5}$	2	1.300889423

#### 4.2Cross-verify with GA results

To further validatEthe engineering applicability of the  $\rho$  p – Eth –  $\eta p$  model in complex multi-layer shielding systems, we conducted cross-validation between its predictions and the NSGA-II genetic algorithm (GA), a mainstream heuristic optimization method. As a black-box optimization strategy, GA can rapidly approach the Pareto front in multi-objective (dose–mass–thickness) frameworks, but it lacks physical interpretability. By comparing GA results with the model's predictions, we can evaluate its forecasting capability in multi-layer structure optimization.

We configured the following GA parameters: population size POP = 20, with each generation producing LAMBDA = 20 offspring; maximum iterations MAXGEN = 10 to balance convergence and computational efficiency; crossover probability CX = 0.7 and mutation probability MUT = 0.3. The encoding method employs a dual-variable representation of 'integer index + continuous thickness', with total thickness capped at  $\leq 1$  cm. We tested structures with 2, 3, and 5 layers. The fitness function combines total surface density minimization and Geant4 re-simulation dose minimization.

GA demonstrates excellent convergence performance: For ten proton energy ranges (40–95 MeV), thEthree-layer structure achieves stable Pareto front in six generations on average. The two-layer structure converges in four generations due to its smaller search space, while the five-layer structure typically requires 8–9 generations owing to higher dimensional complexity. As shown in Table 4, the results reveal optimal shielding material combinations for each proton energy level, specifically the minimum surface density configurations that ensure complete proton shielding.

Table 4 Convergence Results of Optimal Shielding Material Combinations for Genetic Algorithm Under Different Energy Levels

Incident proton	Thickness (cm) + Material			
energy MeV	Five layers	three layers	Two layers	
40	0.08A1 + 0.192C + 0.121A1 + 0.189C + 0.395Be	0.062POLY + 0.772Be + 0.166Al	0.953Be + 0.047C	
50	0.219C + 0.018Pb + 0.03A1	0.505Mg +	0.685Ti +	

	+ 0.555Al + 0.177Cu	0.166Al + 0.329Fe	0.315Be
60	Cu(0.469) + Fe(0.009) + Ti(0.381) + Be(0.053) + Al(0.088)	Fe(0.117) + Mg(0.349) + Fe(0.534)	C(0.442) + Fe(0.558)
70	Pb(0.03) + Ta(0.057) + Ag(0.014) + Ag(0.331) + Ti(0.567)	Cu(0.14) + Tl(0.488) + Al(0.373)	Ag(0.744) + POLY(0.256)
75	W(0.007) + Ag(0.472) + Mg(0.122) + Ag(0.125) + Pb(0.273)	Al(0.403) + Ta(0.301) + Fe(0.296)	Pb(0.427) + Fe(0.573)
80	Cu(0.549) + POLY(0.081) + Mg(0.066) + Ta(0.134) + Ag(0.17)	Cu(0.793) + Fe(0.105) + Ag(0.102)	Cu(0.835) + Fe(0.165)
83	C(0.026) + Ta(0.14) + Cu(0.199) + Ag(0.212) + Fe(0.424)	Mg(0.38) + Be(0.113) + Pt(0.507)	Ag(0.896) + Ta(0.104)
85	W(0.17) + Cu(0.656) + Cu(0.002) + Ag(0.027) + Ti(0.145)	C(0.05) + Ag(0.904) + Au(0.046)	Ag(0.987) + Be(0.013)
90	Ta(0.307) + Ti(0.021) + POLY(0.099) + Be(0.132) + Pt(0.442)	Cu(0.555) + Mg(0.033) + Ta(0.412)	Au(0.24) + Ag(0.76)
95	Pt(0.105) + Al(0.121) + Cu(0.108) + Tl(0.23) + W(0.436)	C(0.119) + Mg(0.124) + Au(0.757)	Au(0.725) + Ti(0.275)

The comparison of proton density  $\rho$  p calculated by the optimal material

combination with the optimal proton density  $\rho$  p obtained by the semi-empirical formula is shown in Table 5.

Table 5 The optimal proton density obtained from the semi-empirical formula and the proton density of the combined type calculated by GA

Proton		$ ho_p$ mol cm $^{-3}$				
Energy	Theoretical Optimum	Five layers	three layers	Two layers		
MeV	Optimum					
83	4.91190253	4.302099745	4.767	4.795		
60	2.756326148	2.898299037	2.685	2.442		
50	1.819119025	1.584012304	1.855	1.652		
40	0.881911903	0.928739016	0.883	0.824		
70	3.693533271	3.270500881	3.35	3.537		
75	4.162136832	4.112862899	3.848	4.016		
80	4.630740394	4.024097778	4.089	4.019		
85	5.099343955	5.156663295	4.533	4.522		
90	5.567947516	6.062900261	5.072	5.333		
95	6.036551078	5.958822396	6.079	6.696		

The comparison results between the model and GA's re-simulated dose are as follows: For thEthree-layer structure, the average prediction error of the model compared to Geant4's re-simulated dose is 6.2%. This configuration demonstrates the best agreement, primarily due to the moderate gradient ρp distribution (0.8–4.5 mol cm<sup>-3</sup>) and diverse layer-thickness combinations (>300), which provide ample optimization space for GA and ensure more stable model predictions. The two-layer structure shows an average error of 8.2%.

With limited combinations, GA is prone to local optima under 1 cm thickness constraints. The significant thickness variability doubles Eth's sensitivity to thickness, while random errors increase. Five-layer structure: The average error is 6.7%. Although there are more layers, the proton density gradient between different layers varies greatly, which may lead to a large variation of the backscatter coefficient  $\beta$  scat and introduce a certain error.

These cross-validation results demonstratEthat our model can maintain dose calculation accuracy within 8% during GA's rapid iterative optimization, fully meeting the forward screening requirements for shielding schemes during spacecraft conceptual design. Although subject to statistical uncertainties and strong dependence on 1cm fixed thickness, the model outperforms traditional black-box optimization methods in computational speed, providing an efficient and physically interpretable tool for preliminary design of complex multi-layer shielding systems.

#### 4.3 Low-Z mass saving and high-Z space saving mechanism

Our  $\rho$  p – Eth –  $\eta p$  ternary coupling model provides the first quantitative explanation of the physical criteria underlying the long-standing 'low-Z mass savings' and 'high-Z space savings' phenomena in deep space radiation protection. This insight offers a universal physical explanation for the 'same surface density-equivalent shielding' debate.

The "mass-saving" advantage of low-Z materials stems from their proton utilization efficiency ( $\eta p$ ). As detailed in Section 4.1,  $\eta p$  follows an exponential decay relationship with  $\rho p$ :  $\eta p = 66.36 \exp(-\rho p / 1.109) + 15.81$ . This indicates that  $\eta p$  increases dramatically when  $\rho p$  is low (i.e., in low-Z materials). Specifically, when  $\rho p < 1 \mod \text{cm}^{-3}$ ,  $\eta p$  can reach  $60-100 \ \text{MeV} \ \text{cm}^{-2} \ \text{mol}^{-1}$ .

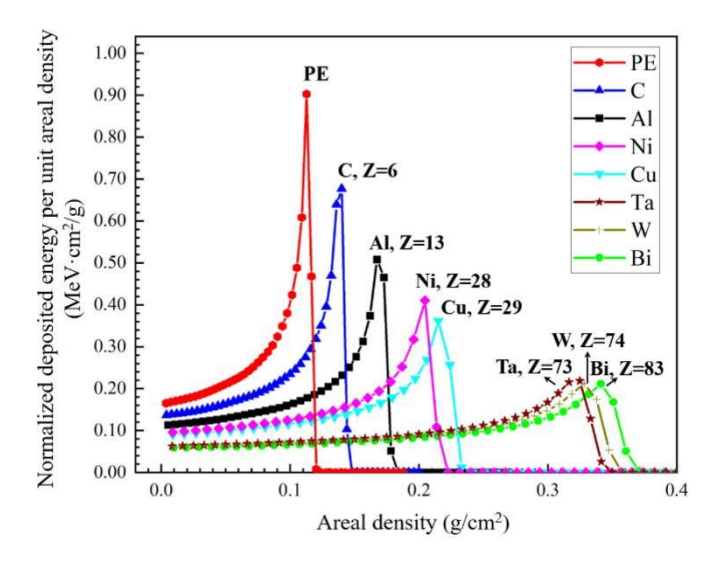


Figure 5: The relationship between the normalized deposited energy of 10MeV monoenergetic protons and proton density variations in different shielding materials

From a material quality perspective, the required mass m for achieving equivalent shielding effectiveness is proportional to Eth and inversely proportional to  $\eta p$ . Low-Z materials exhibit exceptionally high  $\eta p$  in the low  $\rho$  p region, enabling them to absorb more proton energy per unit mass. For instance, when performing shielding tasks with the same surface density  $\rho$  s, the material mass  $m = Eth / (\eta p \cdot constant)$ . Although low-Z materials have relatively lower Eth, their superior  $\eta p$  enables significant mass reduction. This study demonstrates that low-Z materials can reduce mass usage by 35%-55% compared to conventional materials when  $\rho$  p <1 mol cm<sup>-3</sup>. Figure 5 visually illustrates the normalized 10 MeV proton deposition energy variation with surface density and proton density, clearly showing that low-Z materials like PE (polyethylene) and C (carbon) demonstrate higher energy deposition efficiency under identical surface density conditions, thereby validating their mass-saving potential (data and figures cited from Su et al.[20]).

The advantages of high-Z materials are demonstrated through their full absorption threshold (Eth). When  $\rho$  p exceeds 6 mol cm<sup>-3</sup>, although the proton stopping cross-section ( $\eta$ p) drops below 30 MeV cm<sup>-2</sup> mol<sup>-1</sup>, their Eth value increases

significantly. This high Eth enables high-Z materials to effectively block protons with higher energies at the samEthickness. This capability makes them ideal for achieving "ultra-thin shielding" – providing maximum protection within limited spatial constraints.

The findings provide clear guidance for designing multi-layer shielding structures. When the task primarily involves surface density constraints, low-Z systems with ρp <1 mol cm<sup>-3</sup> should be prioritized to achieve maximum mass savings. Conversely, for thickness constraints, strategically stacking high-Z layers can enable ultra-thin shielding, though this approach entails a 30%–60% mass penalty. The optimal solution often lies in multi-layer structures that balance Eth and ηp through ρp gradients (low-Z outer layer + high-Z inner layer), achieving global optimization under the dual constraints of thickness and mass.

#### 5. Conclusion

This study systematically investigates the challenges in deep space radiation shielding design, where the physical mechanisms underlying the "lightweight and efficient" properties of novel low-Z materials remain unclear. This ambiguity has led to excessive reliance on "black-box" algorithms in shielding optimization. We innovatively propose a ternary coupling semi-empirical model, with proton density as the core variable, to correlate it with two key macroscopic shielding performance metrics: full absorption threshold Eth and proton utilization rate  $\eta p$ .

The research yielded three core findings: Through Geant4 simulations and regression analysis, we established a linear positive correlation between Eth and ηp, along with an exponential negative correlation between Eth and ηp. The model demonstrated average prediction errors of 6.2% for Eth and 8.5% for ηp when applied to independent validation set materials. In cross-validation with the NSGA-II genetic algorithm, the dose prediction error for multi-layer structures was controlled within 8.2%, fully meeting the engineering requirements of spacecraft conceptual design. This study provides the first physical quantitative explanation for the intrinsic relationship between "mass savings in low-Z materials" and "space savings in high-Z materials."The study demonstrates that when proton density ρp <1 mol cm<sup>-3</sup>, materials exhibit significant mass savings (35%–55%) due to their exceptional proton utilization efficiency (ηp). Conversely, when ρp> 6 mol cm<sup>-3</sup>, materials demonstrate superior space efficiency through their high full absorption threshold (Eth), which is crucial for achieving ultra-thin shielding. This provides a physically interpretable

universal criterion that resolves the long-standing debate about "equivalent shielding under identical surface density." As a computationally efficient and physically interpretable design tool, this model outperforms traditional black-box optimization methods. It enables rapid and reliable preliminary screening for multi-objective optimization of "surface density-thickness-dose" in deep space missions, directly supporting the engineering design and implementation of next-generation lightweight multi-layer composite shielding systems.

# Reference Documentation

- [1] Durante, M., Cucinotta, F.A. Physical basis of radiation protection in space travel. Reviews of Modern Physics 2011, 83(4), 1245-1281.
- [2] Thibeault, S.A., Kang, J.H., Sauti, G., Park, C., Fay, C.C., King, G.C. Nanomaterials for radiation shielding. MRS Bulletin 2015, 40(10), 836-841.
- [3] Toto, E., Lambertini, L., Laurenzi, S., Santonicola, M.G. Recent advances and challenges in polymer-based materials for space radiation shielding. Polymers 2024, 16(3), 382.
- [4] Naito, M., Kitamura, H., Koike, M., Kusano, H., Kusumoto, T., Uchihori, Y., Kodaira, S. Applicability of composite materials for space radiation shielding of spacecraft. Life Sciences in Space Research 2021, 31, 71-79.
- [5] Guetersloh, S.B., Zeitlin, C., Heilbronn, L., Miller, J., Komiyama, T., Fukumura, A., Bhattacharya, M. Polyethylene as a radiation shielding standard in simulated cosmic-ray environments. Nuclear Instruments and Methods in Physics Research Section B 2006, 252(2), 319-332.
- [6] Wilson, J.W. (Ed.). Shielding strategies for human space exploration. NASA Conference Publication 1997, 3360.
- [7] Toto, E., Lambertini, L., Laurenzi, S., Santonicola, M.G. Recent advances and challenges in polymer-based materials for space radiation shielding. Polymers 2024, 16(3), 382.
- [8] Thibeault, S.A., Kang, J.H., Sauti, G., Park, C., Fay, C.C., King, G.C. Nanomaterials for radiation shielding. MRS Bulletin 2015, 40(10), 836-841.
- [9] Cheraghi, E., Chen, S., Yeow, J.T. Boron nitride-based nanomaterials for radiation shielding: a review. IEEE Nanotechnology Magazine 2021, 15(3), 8-17.
- [10] Azman, M.N., Abualroos, N.J., Yaacob, K.A., Zainon, R. Feasibility of nanomaterial tungsten carbide as lead-free nanomaterial-based radiation shielding. Radiation Physics and Chemistry 2023, 202, 110492.
- [11] Deb, K., Pratap, A., Agarwal, S., Meyarivan, T.A.M.T. A fast and elitist multiobjective genetic algorithm: NSGA-II. IEEE Transactions on Evolutionary Computation 2002, 6(2), 182-197.
- [12] Chen, Z., Zhang, Z., Zhang, Z., Guo, Q., Yu, T., Zhao, P., Liu, Z., He, C. Multi-objective optimization strategies for radiation shielding design with genetic algorithm. Computer Physics Communications 2021, 260, 107267.
- [13] SanScoucie, M.P., Hull, P.V., Tinker, M.L., Dozier, G.V. Lunar habitat optimization using genetic algorithms. NASA Technical Paper 2007,

- NASA/TP-2007-214852.
- [14] Salvat, F. Bethe stopping-power formula and its corrections. Physical Review A 2022, 106(3), 032809.
- [15] Berger, M.J. ESTAR, PSTAR, and ASTAR: Computer programs for calculating stopping-power and range tables for electrons, protons, and helium ions. 1992.
- [16] Suplee, C. Stopping-power & range tables for electrons, protons, and helium ions. 2009.
- [17] MacFadden, N., Peggs, S., Gulliford, C. Development and validation of a Geant4 radiation shielding simulation framework. Brookhaven National Laboratory Report 2018, CBETA/034; BNL-211700-2019-TECH.
- [18] Cucinotta, F.A., Alp, M., Rowedder, B., Kim, M.H.Y. Safe days in space with acceptable uncertainty from space radiation exposure. Life Sciences in Space Research 2015, 5, 31-38.
- [19] Daneshvar, H., Milan, K.G., Sadr, A. et al. Multilayer radiation shield for satellite electronic components protection. Sci Rep 11, 20657 (2021).
- [20] Su, J., Wei, Z., Liu, G., Xu, J., Fei, T., Zhou, B., Han, H. Simulation of radiation environment and design of multilayer radiation shield for orbital exploration of Jupiter. Advances in Space Research 2024, 73(5), 2652-2662.